Microstructure Development during Hot Deformation of Aluminum to Large Strains

TANJA PETTERSEN, BJØRN HOLMEDAL, and ERIK NES

During deformation, the original grains change their shape and the surface area per unit volume increases with strain until a certain critical strain has been reached. The structure of high-angle boundaries has been monitored at increasing strains with the aim of finding the effect of grain breakup and strain-induced boundary migration. It has been found that the distance between the high-angle boundaries does not depend only on geometrical considerations. At high Zener–Hollomon parameters, the distance between the high-angle boundaries was found to be smaller than predicted from geometry, indicating that high-angle boundaries are formed during deformation. In the case of deformation at very low Zener–Hollomon parameters, the distance between the high-angle boundaries was found to be larger than predicted from geometry, which indicates migration of the original grain boundaries in a direction opposite to the one imposed by the deformation. The evolution in grain-boundary structure during deformation has been successfully modeled on the basis of expressions for the grain breakup and restoration reactions.

I. INTRODUCTION

DURING the last few decades, investigations have demonstrated that during deformation of aluminum, a structure consisting primarily of high-angle boundaries can form without recrystallization reactions involving nucleation and growth. Several authors[1–5] observed the development of a structure of equiaxed grains of the same order of magnitude as the subgrains formed in the material. It is commonly observed that the original grains elongate at increasing deformation and that the original grain boundaries develop serrations of the same order of magnitude as the subgrain size. At increasing strain, the distance between the original grain boundaries will eventually be of the order of magnitude of the subgrain size, and a concept termed geometric dynamic recrystallization (GDRX) was suggested by McQueen and co-workers[2,4,5] to account for the further development in the microstructure. The basic idea of GDRX is that when the strain reaches a level where the grain thickness equals twice the subgrain diameter, the concave serrations of the original grain boundary will come into contact and perforate the original grain. The model hence predicts that when this critical strain is reached (the strain where the grains are pinched off), further straining of the material will not lead to an increasing fraction of high-angle boundaries. From this simple picture, the critical strain where the grains are pinched off, and the development of the grain morphology (here, represented by the shortest distance between the original grain boundaries), can easily be predicted solely by using geometrical considerations. Knustad *et al.*[6] and Humphreys and Hatherly[7] reported that the critical strain for pinch off to occur indeed was consistent with this simple idea. During hot deformation, however, grain restoration reactions due to dynamic boundary migration also need to be considered. The objective of this article is to explore the evolution in subgrain/grain structure during hot deformation to large strains at a wide range of temperatures and strain rates.

TANJA PETTERSEN, Senior Engineer, is with R&D Materials Technology, Hydro Aluminium, N-6600 Sunndalsora, Norway. Contact e-mail: Tanja.pettersen@hydro.com BJØRN HOLMEDAL, Post Doc, and ERIK NES, Professor, are with the Department of Materials Technology, Norwegian University Science and Technology (NTNU), N-7034 Trondheim, Norway.

Manuscript submitted May 7, 2003.

II. EXPERIMENTAL METHODS

A. *Material and Processing*

The present work has been concentrated on two different AlMgSi alloys, one AA6060 alloy and one AA6082 alloy, with different manganese content as the main difference. The chemical compositions of the alloys have been obtained by spectrographic analysis, and are listed in Table I.

All alloys have been Direct Chill (DC) cast according to standard industrial practice, and subsequently homogenized to keep the hardening elements in solid solution. The AA6060 alloy was homogenized as follows: heated at a rate of 200 °C/h to 580 °C, kept at this temperature for 8 hours, and finally water quenched. The AA6082 alloy was homogenized for 3 hours at 580 °C and quenched. After homogenization, the material was deformed in torsion at various combinations of strain rate and temperature and to various strains. The specimens used for the torsion tests were machined from cylindrical billets, avoiding the outer 2 cm. The length and the radius of the gage section were 10 and 5 mm, respectively. During deformation, the temperature, the angle of twist, and the torque were sampled in preset time intervals. From these values, the stress, strain, and strain rate were calculated. For further details of the torsion experiment, see Pettersen[8] or Pettersen and Nes.[9]

B. *Microstructural Characterization*

The specimens deformed in torsion were further examined using light optical microscopy (LOM), scanning electron microscopy (SEM), and transmission electron microscopy (TEM). The optical microscope was used to estimate the distance between the high-angle boundaries at the lowest Zener–Hollomon parameters and to give qualitative

information about the deformed structure. Due to its better resolution, the SEM was used to measure the distance between the high-angle boundaries at the higher Zener–Hollomon parameters. It was also used for measuring local orientations and subgrain sizes. The TEM was used for measuring subgrain sizes.

The torsion specimens were examined in the $z\theta$ plane (Figure 1). Care was taken to keep the distance from the center of the specimen to the plane of study the same in all specimens. The LOM and the SEM specimens were ground to a width of 2.6 mm, and hence, all investigations were carried out in a plane at a distance of 4.8 to 5 mm from the center of the gage section. Specimen preparation was carried out by grinding on SiC paper followed by polishing on a cloth with diamond spray. The specimens where then electrolytically polished and the specimens used for optical investigations were in addition anodized in a 5 pct HBF_4 aqueous solution.

Microstructure and texture investigations in the SEM were chiefly carried out as fully automated EBSP measurements (the mapping technique or orientation imaging microscopy (OIM) making a large collection of orientation data feasible). To provide a high density of detected backscattered electrons, the samples were tilted to an angle of 70 deg during operation. The microscope was operated at a high tension of 20 kV, and the specimen was placed at a working distance of 15 mm.

Table I. Chemical Composition of the Investigated Alloys

	Alloying Elements, Given in Weight Percent				
Alloy	Fe	Si	Mg	Mn	Al
AA6060	0.20	0.42	0.49	0.02	balance
AA6082	0.21	0.99	0.65	0.47	balance

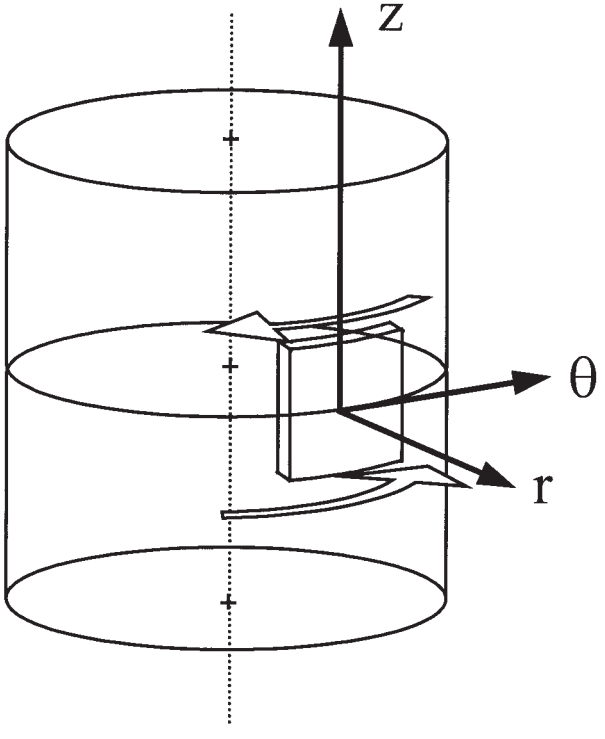

Fig. 1—Schematic illustration of the torsion specimen with the reference directions indicated.

III. RESULTS

The as-cast starting material consisted of a coarse, equiaxed grain structure, and the average mean intercept lengths were measured to be 100 and 61 μm in the AA6060 and the AA6082 materials, respectively. Hot torsion experiments were carried out on the as-cast material, and stress-strain curves were recorded. As the strain increases, the stress first increases to a narrow plateau, followed by a decrease in flow stress of about 20 pct until steady state is reached. The texture was found to change during deformation from a close to random texture at the peak of the stress-strain curve to a texture consisting mainly of the components $\{001\}\langle 110\rangle$ and $\{112\}\langle 110\rangle$ at the strain where the stress-strain curve reaches steady state, and further to an almost pure $\{112\}\langle 110\rangle$-texture at larger strains. The subgrain size was found to increase by about 20 pct from the peak of the stress-strain curve to the final steady state. For further details of the fall in flow stress, the change in texture, and the change in subgrain size, confer Pettersen and Nes.[9]

During deformation, the original grains change their shape, and the surface area per unit volume increases with strain until a certain critical strain has been reached. Using polarized light makes it possible to follow the change in grain shape both with strain, and as effected by the deformation temperature and strain rate. Illustration of such changes are given in Figures 2 and 3 from the AA6060 alloy and the dispersoid containing AA6082 alloy, respectively. It is convenient, in this context, to use the temperature-compensated strain rate (Zener–Hollomon parameter);

$$Z = \dot{\varepsilon} \exp (U/\mathrm{R}T) \qquad [1]$$

where $\dot{\varepsilon}$ is the strain rate, U is an activation energy, R is the gas constant, and T is the temperature. Throughout this work, an activation energy of 156 kJ/mol has been used.

At low strain and low Zener–Hollomon parameters, the original grains could be distinguished as separate entities, separated by the original grain boundaries. The grains are elongated in a direction making a small angle with the shear direction, and the boundaries show a serrated appearance. Increasing the strain, the original grains continue to elongate, and the grain boundaries from opposite sides of the grain will approach each other. Eventually, a structure consisting of small equiaxed "grains" surrounded by high-angle boundaries was observed.

The development with increasing strain at a relatively low Zener–Hollomon parameter is displayed in Figures 2(a) through (c). At a strain of 1, the original as-cast structure is easily recognized, being drawn out in one direction. The equiaxed regions are observed to be formed at a strain of about 3. Increasing the strain further apparently results in no changes in microstructure as followed in the optical microscope. The evolution of the grain-boundary structure was found to be strongly influenced by strain rate and

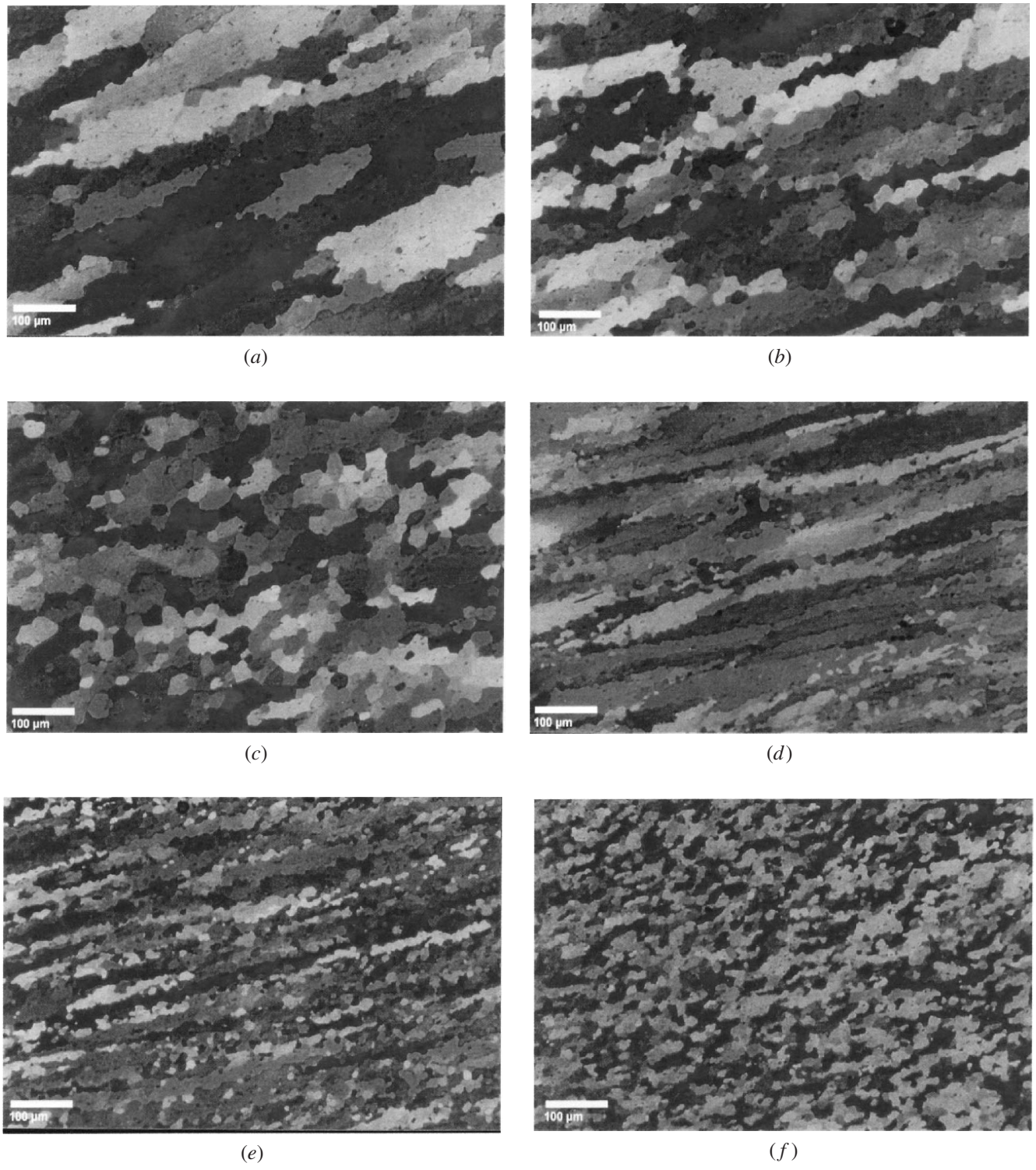

Fig. 2—LOM micrographs from AA6060 specimens deformed in torsion at two different Zener–Hollomon parameters and to various strains. (*a*) through (*c*) are deformed at a strain rate of 1.3 s^{-1} and a temperature of 523 °C; and (*d*) through (*f*) are deformed at a strain rate of 13 s^{-1} and a temperature of 486 °C: (*a*) strain = 1, (*b*) strain = 2, (*c*) strain = 3, (*d*) strain = 1, (*e*) strain = 2, and (*f*) strain = 25.

temperature (Z). In the high Z material, the microstructure reaches the state of small equiaxed grains partly surrounded by high-angle boundaries at a lower strain than the low stress microstructure. For a Zener–Hollomon parameter of $7 \cdot 10^{11}$ s^{-1}, a structure consisting of small equiaxed grains was found to develop at a strain of about 2. A more detailed description of the substructure evolution can be achieved by applying the EBSD technique in SEM. Figures 4(a) through (c) illustrate the subgrain/grain structure and corresponding pole figures at different strain levels (1, 5, and 25) revealed by orientation imaging microscopy (OIM); for a detailed description of the evolution in deformation texture, see

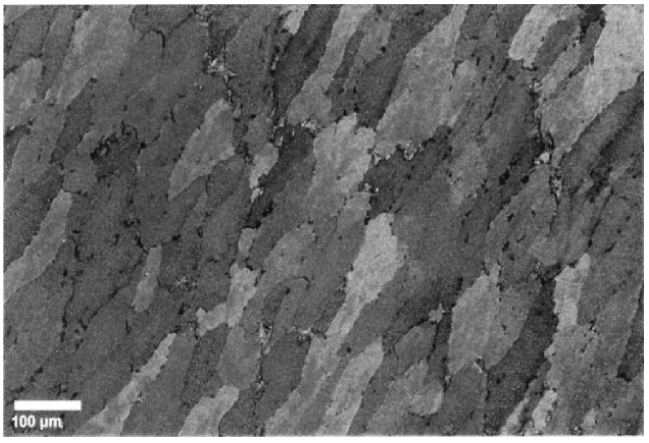

(*a*)

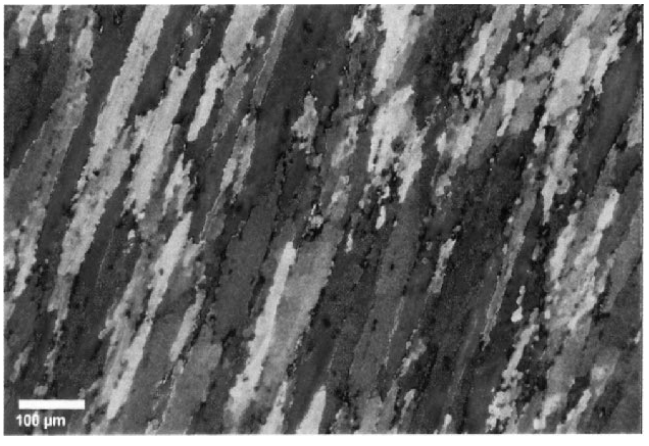

(*b*)

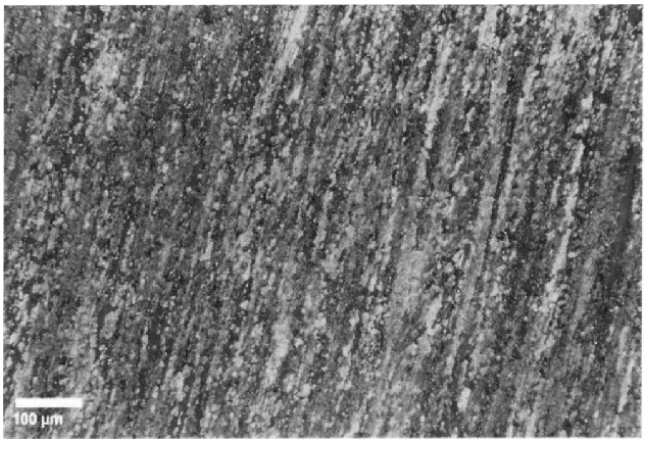

(*c*)

Fig. 3—LOM micrographs from specimens of the AA6082 alloy deformed in torsion with deformation conditions as follows: (*a*) temperature = 540 °C, strain rate = 0.0025 s^{-1}, ($Z = 3 \cdot 10^7$ s^{-1}); (*b*) temperature = 523 °C, strain rate = 1.3/s, ($Z = 2 \cdot 10^{10}$ s^{-1}); (*c*) temperature = 480 °C, strain rate = 25 s^{-1} ($Z = 2 \cdot 10^{12}$ s^{-1}). All the specimens were deformed to a strain of 1.5.

Reference 9. A more quantitative representation of the change in boundary structure is illustrated by the corresponding misorientation distributions in Figures 5(a) through (c). Note that the nature of the boundary structure changes from being of a sub-boundary type at small strains to containing a dominating fraction of high-angle boundaries at large strains.

Figure 3 demonstrates the changes in grain morphology with the Zener–Hollomon parameter in the alloy AA6082. At the lowest Zener–Hollomon parameter, the original grain structure is easily recognized. The structure consists of large elongated bands with apparently no microstructure inside the bands (this was also confirmed by mapping investigations). The original grain boundaries are only slightly serrated, and large areas of nearly straight boundaries could be observed. At a Zener–Hollomon parameter of $2 \cdot 10^{10}$/s a different microstructure appears. The original grains can still be recognized, however, not as easily as for the low-Z material. Deforming the material at even higher Zener–Hollomon parameters, the material shows a completely different microstructure. The original grains can no longer be distinguished, and the microstructure consists of small equiaxed grains apparently surrounded by high-angle boundaries, similar to that found at high strains for specimens deformed at lower Zener–Hollomon parameters.

As a quantitative measure of the change in the grain structure, the distance between high-angle boundaries (measured in the axial direction, D_z, Figure 1) in the microstructure after deformation was measured both in the optical microscope and in the scanning electron microscope. When SEM measurements and light optical measurements were carried out on the same specimens, it was found that the SEM measurements gave lower values of the mean axial width. The effect of this is found to decrease with decreasing Zener–Hollomon parameter. The results from the measurements of axial width are displayed in Figure 6.

It follows from the figure that deformation at Z levels above $\sim 10^{10}$ s^{-1} is associated with rapid break up of the grains, which results in a steady-state equiaxed structure for deformation above a strain of about 3 to 4. At lower Zener–Hollomon parameters, other mechanisms are apparently dominating, and the axial width stabilizes at a value well above the value predicted from the geometry. This is illustrated by the specimens deformed at $Z = 2 \cdot 10^8$ s^{-1}. At a strain of 10 ($Z = 2 \cdot 10^8$ s^{-1}), the axial width is even seen to increase.

The effect of dispersoids on this break-up pattern is also illustrated by Figure 4. As can be clearly seen from the figure, the dispersoids result in a decrease in axial width of the deformed grains. The effect is largest at the lowest Zener–Hollomon parameters, and the dispersoids are seen to suppress the boundary migration phenomena observed in the 6060 alloy at $Z \sim 10^8$ s^{-1}.

IV. DISCUSSION

A. *The Shape Changes of the Grains during Deformation*

Using the GDRX model, the distance between the original grain boundaries can easily be predicted solely by using geometrical considerations. Imagine two lines drawn parallel to the z-axis (Figure 1) at the surface of the torsion specimen before deformation. The distance between the two lines is set to be D_0, and a cubic grain with edges of length D_0 is placed between the lines. Deforming the specimen in torsion to an angle of θ, the length of the two lines has increased to $L(\theta)$, the geometry of the inserted grain has

(*a*)

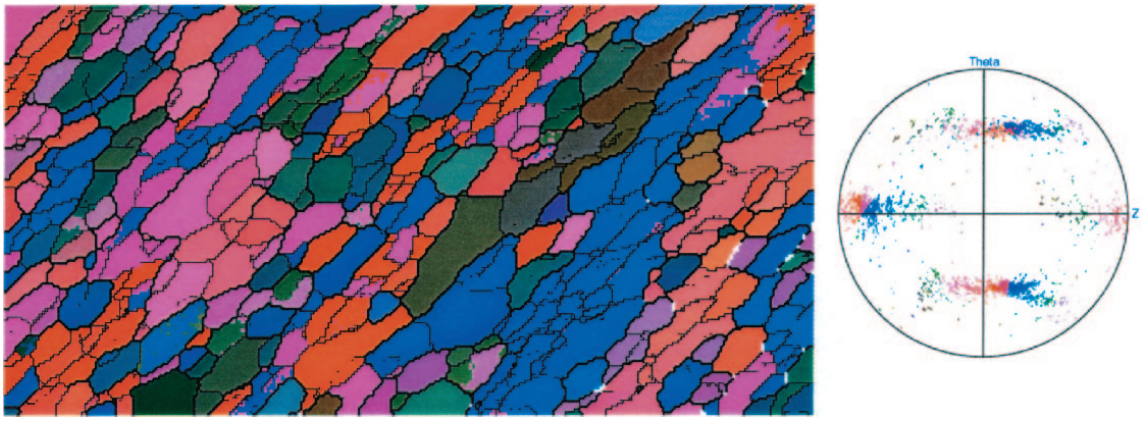

(*b*)

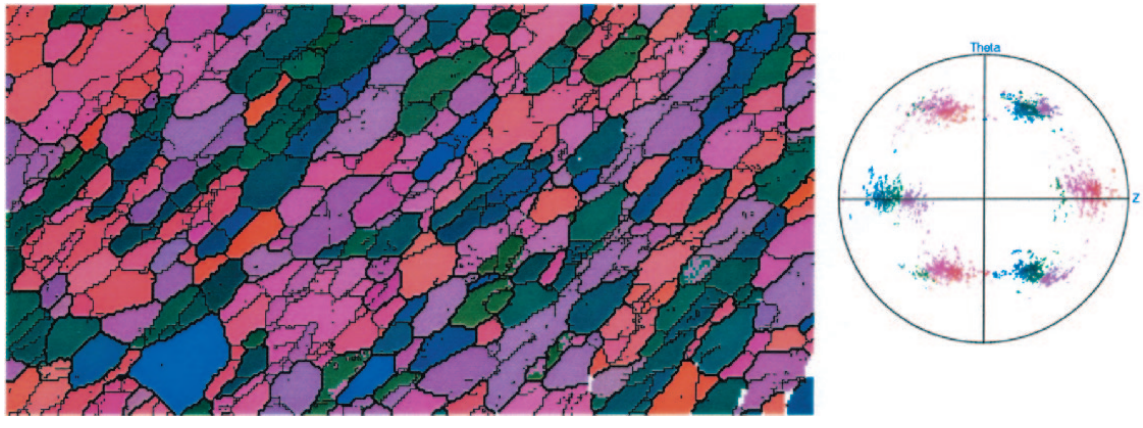

(*c*)

Fig. 4—OIMs and corresponding (200) pole figures showing AA6060 deformed at $Z = 7 \cdot 10^{11}$ s^{-1} and to strains of (*a*) $\varepsilon = 1$, (*b*) $\varepsilon = 5$, and (*c*) $\varepsilon = 25$. The boundaries with misorientation greater that 15 deg are marked with heavy lines and the boundaries with misorientations ranging from 1.5 to 15 deg are marked with thin lines.

changed, and, assuming conservation of volume, the distance between the lines has decreased to

$$D_{GSC} = D_0 \frac{L}{L(\theta)} \quad [2]$$

Simple geometry means that for a torsion specimen of length L and radius R, the length $L(\theta)$ is given by $L(\theta) = \sqrt{L^2 + R^2\theta^2}$, which, when converting the angle of twist to strain (ε), leads to the following expression for the distance between the high-angle boundaries:

$$D_{GSC} = \frac{D_0}{\sqrt{1 + 3\varepsilon^2}} \quad [3]$$

This expression is similar to the expression derived by Knustad *et al.*[6] As pointed out by Knustad *et al.*, the expression is only valid for strains below the critical strain necessary to

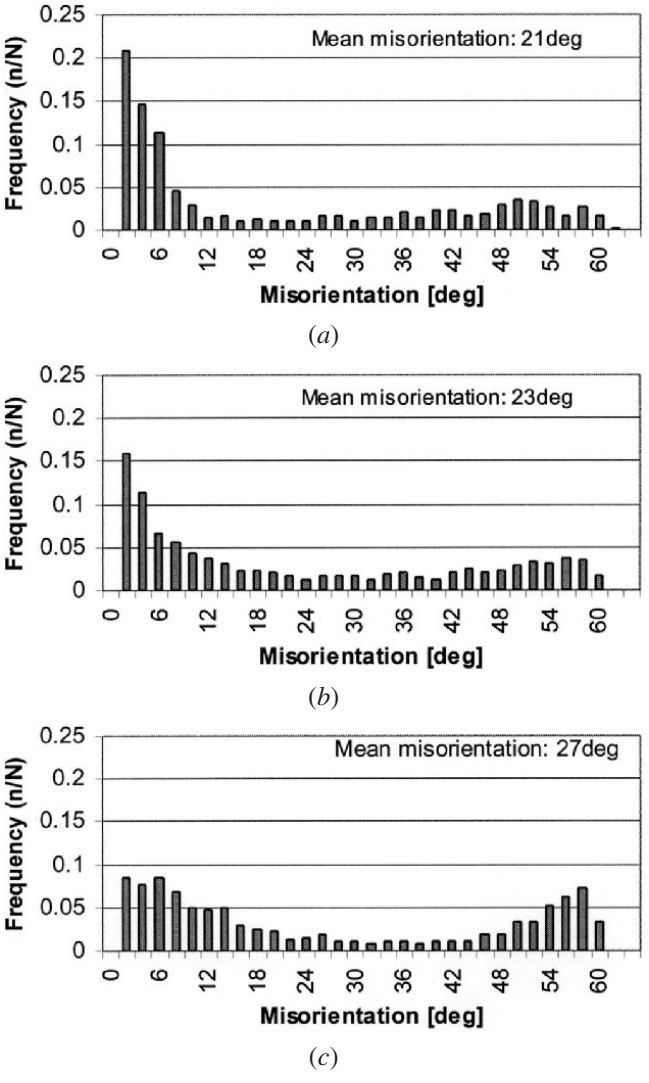

Fig. 5—Boundary misorientation histograms for AA6060 deformed at $Z = 7 \cdot 10^{11}$ s^{-1} to strains of (*a*) $\varepsilon = 1$ (4207 measurements), (*b*) $\varepsilon = 5$ (2890 measurements), and (*c*) $\varepsilon = 25$ (2912 measurements).

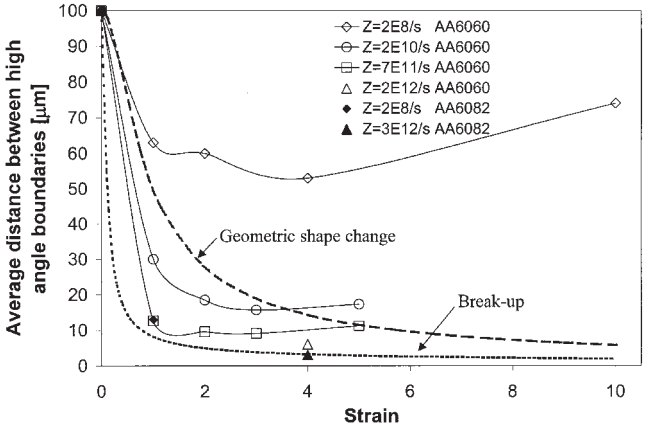

Fig. 6—Axial band width (measured as linear intercepts) as a function of strain. The white symbols show the values obtained from the AA6060 alloy, and the black symbols show the AA6082 alloy, for the values of *Z* given. Light optical microscopy has been used in one case ($Z = 2 \cdot 10^8$ s^{-1}, AA6060).

pinch off the grain. Humpreys and Hatherly[7] considered deformation in compression and obtained a corresponding expression, indicating an exponential fall in the average distance between the high-angle boundaries consistent with their mode of deformation. It follows that the critical strain becomes smaller in compression than in torsion. In the following, Eq. [3] is used for the geometric shape change of a grain. The critical strain, ε_c, is easily found from the preceding expression to be

$$\varepsilon_C = \sqrt{\frac{1}{3}\left[\left(\frac{D_0}{2\delta}\right)^2 - 1\right]} \approx \frac{D_0}{2\sqrt{3}\cdot\delta} \qquad [4]$$

where δ is the subgrain size.

In the present work, optical investigations of the material deformed in torsion to a large extent confirmed the general predictions of the geometric dynamic recrystallization model. At low strains, the grains elongated and the large-angle boundaries were seen to be slightly serrated. At increasing strains, the grain boundaries continued to elongate, and eventually a structure of equiaxed grains surrounded by high-angle boundaries developed. The model of geometric dynamic recrystallization, however, was not able to predict all changes seen in the present study. From Eq. [3], it is deduced that, according to the model, the distance between the high-angle boundaries in the *z* direction is dependent only on the initial grain size and the strain. However, the experimental results of the present investigation clearly demonstrate that the distance between the high-angle boundaries is dependent on both alloy composition and the Zener–Hollomon parameter in addition to the strain. This means that while the GDRX model predicts that the high-angle boundaries in the structure exclusively originate from the grain boundaries present in the structure before deformation, the present results tend to show that in some cases, high-angle boundaries also form during deformation. This is shown in Figure 6, where deformation at *Z* levels above $\sim 10^{10}$/s is associated with rapid breakup of the grains, which results in a steady-state equiaxed structure for deformation above a strain of about 3 to 4. From the optical investigation, it was also found that for the case of deformation at very low Zener–Hollomon parameters, the distance between the high-angle boundaries was found to be larger than that predicted from Eq. [3], the broken line in Figure 6. An illustration of this is shown in this figure, where the average distance between high-angle boundaries is plotted as a function of strain. Similar results have been reported by Vatne and co-workers.[10,11]

The effect of dispersoids on this break-up pattern is illustrated by Figure 6. As can be seen from the figure, the dispersoids result in a decrease in axial width of the deformed grains. The effect is apparently largest at the lowest Zener–Hollomon parameters, and the dispersoids are seen to suppress the boundary migration phenomena observed in the AA6060 alloy at $Z \sim 10^8$/s.

It follows from the present results that the evolution of grain structure during hot deformation is the combined result of three different mechanisms:

1. geometric shape change due to the imposed straining;
2. introduction of new high-angle boundaries, grain breakup; and
3. boundary migration, dynamic grain growth.

Geometric shape change due to imposed straining has already been treated previously, and the predicted shape change due to geometrical considerations only is plotted in Figure 6.

1. *Grain breakup*

At relatively high Zener–Hollomon parameters, the average distance between the high-angle boundaries is lower than predicted by pure geometric considerations. Correspondingly, it can be concluded that high-angle boundaries are formed during deformation. There are essentially two mechanisms for creating new high-angle boundaries during deformation: grain breakup and the possible formation of new high-angle boundaries from already existing low-angle boundaries.

The most well-known mechanism for the introduction of new grain boundaries is the one treated by Dillamore and Katoh.[12] During deformation, it might happen that one single grain splits into two (or more) parts that take various deformation paths and rotate toward different, but stable and energetically equivalent end orientations. In the region between the crystals of different orientation, a high-angle boundary is formed. The splitting of a grain in this manner is expected to lead to continuous bands of subgrains with similar orientation, and the grain boundary produced is expected to be relatively straight.

In the high-angle boundary structure found in the present investigation, short segments of high angle of misorientation, not separating different grains, were sometimes found. This phenomenon has been treated by Huges *et al*.,[13,14] who suggested that during deformation, some subgrain boundaries might accumulate dislocations and transform into high-angle boundaries.

2. *Dynamic grain growth*

When deforming a material the density of high-angle boundaries will increase both for geometric reasons and due to the break-up phenomena, as explained previously. On the other hand, this grain refinement will introduce sharp boundary curvatures, which in turn, leads to restoration reactions. That is, there will be forces acting on the grain boundaries opposite to the imposed deformation, with the aim of reducing the density of high-angle grain boundaries. Such a restoration reaction is consistent with the present results (Figure 6), which show that after some strain, a steady-state grain size is established. As expected, the size of this steady-state grain size depends on the temperature and strain rate or the Zener–Hollomon parameter. A simple model for the evolution in the grain structure is presented in Section B.

B. *Modeling the Evolution in Grain Structure during Hot Deformation*

Provided that expressions for both the grain refinement and restoration phenomena can be formulated, then the grain evolution is obtained by solving a differential equation of the form

$$\frac{dD}{d\varepsilon} = \frac{dD^-}{d\varepsilon} + \frac{dD^+}{d\varepsilon} \qquad [5]$$

where $dD^-/d\varepsilon$ refers to athermal grain refinement due to a combination of geometric shape changes and break-up reactions, and $dD^+/d\varepsilon$ represents restoration reactions that stimulates grain growth. No theory has been developed to predict the grain refinement in quantitative or analytical terms. However, on the assumption that the grain shape changes observed in the dispersoid containing AA6082 alloy (Figure 6) are nearly athermal in nature (restoration reactions inhibited by the Zener drag), the following empirical relationship is proposed:

$$\frac{dD^-}{d\varepsilon} = f(\varepsilon) \cdot nAD\left(\frac{D}{D_0}\right)^{1/n} \qquad [6]$$

By selecting $A = 278$, $n = 0.5$ (on the origin of this n value, see subsequent discussion), and $f(\varepsilon) = 1 - (\frac{1}{4}\varepsilon + 1)\exp(-2\varepsilon)$, the grain refinement curve (dotted line) in Figure 6 is obtained. Grain growth is driven by boundary curvature forces, the rate of which, on parametric form, can be written:

$$\frac{dD^+}{dt} = m\left(\frac{4\gamma_{GB}}{D}\right) \qquad [7]$$

Here, m is the grain-boundary mobility and the term in parentheses represents the driving pressure for grain growth, where γ_{GB} is the grain-boundary energy. The grain-boundary mobility is written as

$$m = \frac{m_0 \mathbf{b}^4 \nu_D}{\mathrm{k}T}\exp\left(-\frac{U}{\mathrm{k}T}\right) \qquad [8]$$

where m_0 is a constant, $\mathbf{b}$ is the magnitude of the Burgers vector, k is the Boltzmann's constant, and ν_D is the Debye frequency. By replacing dt in Eq. [7] by $d\varepsilon/\dot{\varepsilon}$, this equation takes the form

$$\frac{dD^+}{d\varepsilon} = \frac{B}{\mathrm{k}T}\left(\frac{1}{ZD}\right), \text{ where } B = 4m_0\mathbf{b}^4\nu_D\gamma_{GB} \qquad [9]$$

By combining Eqs. [5], [6], and [9], the evolution in grain structure can be obtained for a given combination of strain rate and temperature. This evolution equation has to be solved numerically. However, a solution for the steady-state grain size, D_{ss}, is easily found from Eq. [5] for the condition $dD/d\varepsilon = 0$; *i.e*.,

$$\frac{D_{ss}}{D_0} = CZ^{\frac{n}{2n+1}}, \text{ where } C = \left(\frac{B}{nA\mathrm{k}TD_0^2}\right)^{\frac{n}{2n+1}} \qquad [10]$$

This exponential decay in the grain size as a function of Z is nicely confirmed by the experimental observations in Figure 7(a), where $log\ (D_{ss}/D_0)$ is plotted as a function of log Z. This plot gives $n = 1/2$ and $C = 65$. A complete solution of Eq. [5] for the conditions investigated gives the results shown in Figure 7(b), which illustrates that the present phenomenological approach provides a reasonable prediction of the evolution in grain structure for a range of temperature and strain rate combinations. A comment is needed regarding the reversion of the observed grain refinement toward large strains, as shown in Figures 6 and 7. These diagrams show that the steady-state grain size starts to increase beyond a critical strain level. This effect is assumed to be associated with the continued increase in the area fraction of high-angle boundaries in the substructure with increasing strain, a consequence of which is an associated increase in the average boundary mobility.

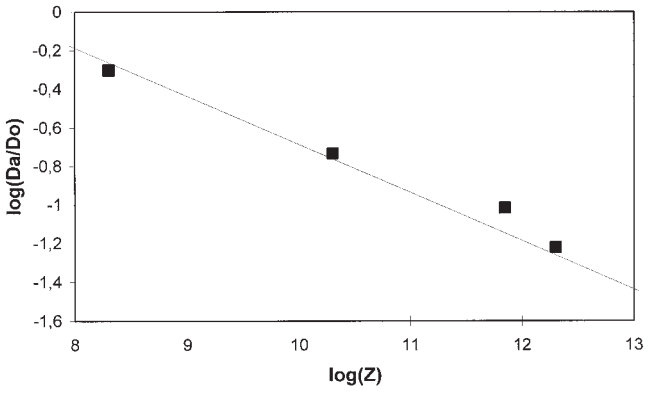

(*a*)

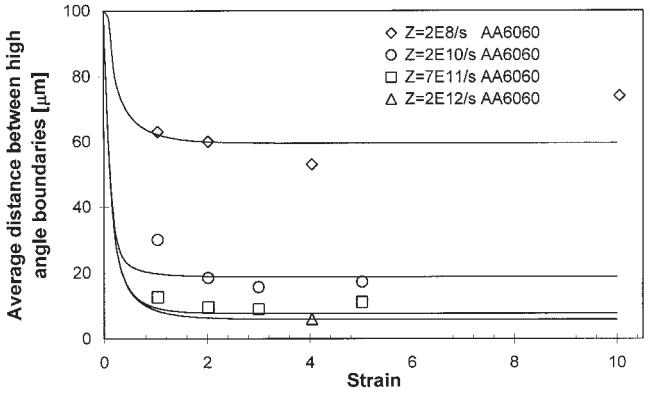

(*b*)

Fig. 7—(*a*) The logarithm of the normalized axial band width as a function of the Zener–Hollomon parameter (*Z*). (*b*) The results of modeling the grain-boundary spacing for the values of *Z* given. Experimental data from the 6060 alloy.

V. CONCLUSIONS

During deformation in torsion, the original grains change their shape, and at large strains, a microstructure consisting of small equiaxed grains surrounded by high-angle boundaries is formed. The distance between the high-angle boundaries has in the present investigation been found to be the result of geometric shape change, grain breakup, and strain-induced boundary migration. The evolution in grain-boundary structure during deformation has been successfully modeled on the basis of expressions for the grain break-up and restoration reactions.

ACKNOWLEDGMENTS

Thanks are due to Hydro Aluminium for financial support, and for providing the material. The present work has benefited from a major European Community programme; the Brite-Euram project REAP, Project No. BE96-3364.

REFERENCES

1. F.J. Humphreys: *Proc. ICOTOM*, 1982, vol. 6 (1), pp. 625-30.
2. H.J. McQueen, O. Knustad, N. Ryum, and J.K. Solberg: *Scripta Metall.*, 1985, vol. 19, pp. 73-78.
3. M.E. Kassner and M.E. McMahon: *Metall. Trans. A*, 1987, vol. 18, pp. 835-46.
4. J.K. Solberg, H.J. McQueen, N. Ryum, and E. Nes: *Phil. Mag. A*, 1989, vol. 60, pp. 447-71.
5. H.J. McQueen, J.K. Solberg, N. Ryum, and E. Nes: *Phil. Mag. A*, 1989, vol. 60, pp. 473-85.
6. O. Knustad, H.J. McQueen, N. Ryum, and J.K. Solberg: *Practical Metallogr.*, 1985, vol. 22, pp. 215-29.
7. F.J. Humphreys and M. Hatherley: *Recrystallization and Related Annealing Phenomena*, Pergamon Press, Oxford, United Kingdom, 1995.
8. T. Pettersen: Ph.D. Thesis, Norwegian University of Science and Technology, Trondheim, Norway, 1999.
9. T. Pettersen and E. Nes: *Metall. Mater. Trans. A*, 2003, vol. 34A, pp. 2727-36.
10. H.E. Vatne: PhD Thesis, Norwegian University of Science and Technology, Trondheim, 1995.
11. H.E. Vatne, R. Shahani, and E. Nes: *Acta Mater.*, 1996, vol. 44, pp. 4447-61.
12. I.L. Dillamore and H. Katoh: *Met. Sci.*, 1974, vol. 8, pp. 73-83.
13. D.A. Huges: *Proc. 16th Risø Int. Symp. on Material Science*, 1995, Risø National Laboratory, Roskilde, Denmark, pp. 63-85.
14. D.A. Huges and A. Godfrey: *Hot Deformation of Aluminium Alloys II*, The Minerals, Metals & Materials Society, Warrendale, PA, USA, 1998, pp. 23-36.